The FASEB Journal express article 10.1096/fj.00-0547fje. Published online February 20, 2001.

Amphiphilic, tri-block copolymers provide potent, membrane-targeted neuroprotection

Jeremy D. Marks*, Chien-yuan Pan[†], Trevor Bushell[†], William Cromie[‡], and Raphael C. Lee[‡]

Departments of *Pediatrics, [†]Physiological & Pharmacological Sciences, and [‡]Surgery, University of Chicago, 5841 S. Maryland Avenue, Chicago, Ill.

Corresponding author: Jeremy D. Marks, Department of Pediatrics, MC 6060, University of Chicago, 5841 S. Maryland Ave., Chicago, IL 60637. E-mail:
j-marks1@uchicago.edu

ABSTRACT

Excitatory amino acid receptor activation and reactive oxygen species production are important mediators of neuronal death following acute brain injury and can lead to loss of membrane integrity. Poloxamer 188 (P188) is an amphiphilic, polyethylene-polypropylene-polyethylene copolymer that restores plasma membrane integrity of nonneuronal cells following membrane injury. Here, we demonstrate that P188 provides profound protection of hippocampal and cerebellar neurons following severe excitotoxic and oxidative injury *in vitro*, through membrane-targeted mechanisms. Widespread death of cultured hippocampal neurons observed 48 h after *N*-methyl-D-aspartate (NMDA) exposure was prevented by incubation of neurons in P188 following NMDA. P188 provided similar neuroprotection from kainate, menadione, and *tert*-butyl-hydroperoxide, but not from staurosporine. P188 application did not alter either NMDA receptor function or NMDA-induced $[Ca^{2+}]_i$ increases. Whole-cell capacitance measurements revealed that P188 application increased cell surface area, consistent with its insertion into the plasma membrane. Following plasma membrane electroporation, P188 arrested loss of intracellular contents, which demonstrated direct restoration of plasma membrane integrity following physical disruption. Measurements of oxidized C11-BODIPY$^{581/591}$ fluorescence demonstrated that P188 blocked lipid peroxidation. These observations demonstrate that amphiphilic tri-block copolymers provide strong, membrane-targeted neuroprotection and represent a novel approach to the treatment of acute neuronal injury.

Key words: poloxamer • *N*-methyl-D-aspartate • excitotoxicity • lipid peroxidation • electroporation • capacitance

Activation of receptors for glutamate plays a central role in neuronal death following hypoxia-ischemia/reperfusion, hypoglycemia, or trauma (1). Activation of the *N*-methyl-D-aspartate (NMDA) receptor subtype is an important mediator of neuronal death, and this mechanism depends on receptor-linked increases in free intracellular Ca^{2+} concentration $([Ca^{2+}]_i)^2$. In addition to depleting ATP as a result of energy-requiring Ca^{2+} extrusion[3], NMDA-induced $[Ca^{2+}]_i$ influx increases production of reactive oxygen species (4, 5), inducing cellular damage via single-strand DNA breaks, protein oxidation, and lipid peroxidation (6). Lipid peroxidation, along with Na^+ and Cl^- influx-mediated osmotic swelling, damages the plasma membrane, with loss of plasma membrane integrity, subsequent loss of intracellular contents, and neuronal death (6, 7). Loss of membrane integrity therefore occurs as a result of attacks on the plasma membrane by multiple mechanisms, and is a pivotal event in necrotic cell death.

Loss of membrane integrity is also an important mechanism of death in Ca^{2+}-independent injury of other cell types, including muscle cells and fibroblasts. Cell death can be markedly reduced by amphiphilic, tri-block copolymers following Joule heating (8), electrical injury (9), or radiation injury (10). These water-soluble, nonionic surfactants are composed of two hydrophilic chains of polyethylene oxides (PEO) separated by a hydrophobic chain of polypropylene oxides (PPO). Differential scanning calorimetry of vesicles composed of phospholipid and tri-block copolymer demonstrates that these compounds incorporate into lipid bilayers (11). Significant cellular protection has been reported with Poloxamer 188 (P188), a tri-block copolymer (mw 8,400) containing a central block (mw 1,750) of 29 PPO moieties and 2 peripheral blocks (mw 3,500) of 38 PEO moieties each (**Fig. 1**). P188 blocks electropermeabilization-induced loss of intracellular contents from skeletal muscle *in vivo* and *in vitro* (12), and enhances functional recovery of fibroblasts from lethal heat shock (13). PEO-PPO-PEO copolymers markedly improve survival of nonneuronal cells following injury in which loss of membrane integrity plays an important role. However, the potential of these molecules in protecting neurons from insults resulting in necrosis has not been investigated.

We investigated whether Poloxamer 188 protects neurons *in vitro* from necrosis by measuring neuronal survival following severe excitotoxic and oxidative injuries. After finding marked neuroprotection, we performed experiments to elucidate the mechanisms mediating this neuroprotection. We measured changes in whole-cell capacitance to assess P188-induced increases in cell surface area, determined the effect of P188 on neuronal membrane integrity following acute disruption, and measured P188 effects on induced lipid peroxidation.

MATERIALS AND METHODS

Hippocampal neurons *in vitro*

Fetal hippocampal neurons were dissociated and maintained *in vitro* according to the method of Banker and Cowan (14). Briefly, astrocyte-enriched glial cultures from 2 d-old rats were plated onto 35-mm petrie dishes in Dulbecco's modified Eagle's medium (DMEM) containing fetal bovine serum (10%) and allowed to proliferate to confluence at 37°C in 5% CO_2. The culture media was replaced with DMEM containing horse serum (10%), N2 supplement (Life Technologies, Rockville, Md.) and ovalbumen (1 mg/ml). One day later, fetal rats from timed pregnancies were killed at 17 day's gestation. Following trypsin digestion, hippocampi were mechanically dissociated and plated at 60,000 cells/ml onto poly-*L*-lysine-coated coverslips containing wax feet on each corner. Coverslips were placed face-down into petrie dishes containing glia and glia-conditioned media and incubated at 37°C in 5% CO_2. Cytosine-β-D-arabinofuranoside was added 24 h later to inhibit glial growth. Neurons were studied at 14 d *in vitro*.

Induction of neuronal death

Dissociated fetal hippocampal neurons were used for toxicity studies, except for studies of kainate toxicity, in which cultures of fetal Purkinje neurons were used. Coverslips containing neurons were placed in saline buffered with N-[2-hydroxyethyl]-piperazine-N'-[2-ethanesulfonic aid] (HEPES), to which the toxin of interest had been added. The composition of the saline was (in millimolars): NaCl 125 , KCl 3.0, $MgCl_2$ 1.3, $CaCl_2$ 2.4 , glucose 10, HEPES 20 (pH 7.40). For studies of NMDA toxicity, the saline contained glycine (10 μM) and 0 Mg^{2+}. The following toxins were used: NMDA (300 μM), kainate (100 μM), menadione (30 μM), tert-butyl-hydroperoxide (100 μM), and staurosporine (200 nM). Neurons were toxin-exposed for 15 min. Sister cultures were exposed to saline alone. Coverslips were placed back with their glial co-cultures, and neuronal death assessed 48 h later.

Assessment of neuronal death

Neuronal death following toxin exposure was quantified with a fluorescent live-dead cell assay. Live neurons were identified by the presence of endogenous esterase activity, as demonstrated by their conversion of nonfluorescent calcein-acetoxymethyl ester (calcein-AM) to fluorescent calcein. Dead neurons were detected with a membrane-impermeable nucleic acid stain (propidium iodide) to identify cells without intact membranes. Neurons were incubated for 5 min in calcein-AM (1μM) and propidium iodide (1 μM). Cells illuminated with 480-nm light, and the resultant red (propidium iodide) and green (calcein) fluorescence observed through a 40× oil objective, appropriate polychroic beam splitter and emission filters (83000 series, Chroma Technology, Brattleboro, Vt.). Neurons located within nine adjacent high-power fields in a 3 ×3 grid were counted in each coverslip. Neuronal mortality was calculated as a ratio of dead neurons to total neurons, and expressed as a percentage. A minimum of six coverslips per condition was counted, and the results were summed. Statistical analysis was performed with logistic regression, and significant differences between groups assessed with the likelihood ratio test.

Time-lapse studies

Neurons cultured on coverslips were placed in a low volume, glass-covered recording chamber (Warner, New Haven, Conn.) on the microscope stage, and perfused (1–2 ml/min) with HEPES-buffered saline heated to 34.5° ± 0.2 C. Drugs were diluted in perfusate in separate syringes connected to a manifold. After fluid changes, the contents of the recording chamber were completely exchanged within 3–4 s. Neurons were observed with an inverted microscope (Nikon, Japan) and imaged with a cooled CCD camera (Photometrics, Tucson, Ariz.) connected to a computer workstation running Metafluor imaging software (Universal Imaging, Downington, Pa.). Images were formed by using a 40×, 1.3 NA oil-immersion objective. Fluorescent dyes were excited via epifluorescence microscopy from a 75W Xenon source, the intensity of which was decreased with neutral density filters. Images of a drop of dye-free perfusate were used as a background image. Nonuniform illumination in the imaging system was corrected by dividing each image by a fluorescent image of a homogenous, uranium oxide slide, and the resultant image was scaled.

Calcium imaging

$[Ca^{2+}]_i$ was measured with Fura-4F (5 μM). Prior to study, cultures were loaded for 1 h at 32° C with calcium reporting dye diluted in bicarbonate-buffered saline. Following loading, cultures were washed in HEPES-buffered saline for at least 15 min to ensure complete hydrolysis of the AM ester form of the dye. Intracellular dye was sequentially excited at 340 nm and 380 nm every 20 s by means of narrow band-pass optical filters, and the emitted light imaged in a band centered around 535 nm. Ratio images were calculated from background-subtracted, shading-corrected images. $[Ca^{2+}]_i$ responses of individual neurons were quantified as the mean ratio within a region of interest on an image-by-image basis and were plotted as a function of time. Peak $[Ca^{2+}]_i$ responses for each neuron were averaged across cells and trials and compared across treatments by using ANOVA for repeated measures. Post hoc comparisons of means were performed according to Scheffe (15). Differences were considered significant if $p < .05$.

Electrophysiology

Whole-cell patch clamp data were obtained by using an Axopatch 1-D amplifier controlled by pClamp software (Axon Instruments, Foster City, Calif.). Voltage-clamp records were filtered at 2 kHz, digitized at 100 kHz, and stored on FM tape. Patch pipettes (3–8 MΩ) were pulled from hematocrit tubing. Pipette solutions contained (in millimolars): K-gluconate 140, HEPES 10, EGTA 10, Mg_2ATP 5, $MgCl_2$ 2 (296 mOsm). Extracellular saline contained (in millimolars): NaCl 144, HEPES 10, $CaCl_2$ 2, $MgCl_2$ 1, KCl 3, glucose 10, (312 mOsm, pH 7.40). NMDA solutions were made in Mg^{2+}-free saline containing glycine (10 μM). NMDA were applied by changing the bathing solution.

Electroporation

Cultured hippocampal neurons were incubated in HEPES-buffered saline containing calcein-AM (1 μM) for 15 min, then washed in calcein-free saline to ensure complete hydrolysis of the acetoxy-methyl ester. Coverslips containing neurons were placed in a perfusion chamber that had been modified so that two flat band platinum electrodes (1-cm wide) projected into the media, separated by a fixed distance of 2 mm. The depth of the perfusate was 3 mm. Images were acquired every 4 s. Regions of interest were defined around each cell, and mean fluorescence within each region plotted as a function of time. Following baseline imaging, neurons were stimulated with a 1 s train (5 Hz) of 4 ms current pulses (see below), and images continued to be acquired every 4 s. For each cell, changes in mean fluorescence over time was expressed as percentage change from the mean of the 5 points immediately before the electroporation.

Current was delivered to the cells via a power supply (Kepco BPO 200-1M, Flushing, N.Y.) controlled by a pulse generator (HP222A, Hewlett Packard, Santa Clara, Calif.). Stimulation consisted of a single train (5 Hz) of square wave pulses (4-ms duration, 200V). We used an inductance coil connected to an oscilloscope and measured pulse amplitude at 0.5 A. The electrical field strength (*E*) applied to the cells in the chamber during each pulse was calculated using the formula,

EQUATION 1

where *J* is the current density and σ is the conductivity of the buffer. Because the surface area of the electrode within the chamber was 0.3 cm^2 , the current density was 1.67 A/cm^2. Using 0.01 S/cm as the conductivity of physiologic saline (16), *E* = 167 V/cm.

The transmembrane potential (V_{membr}) induced by each pulse to the neurons in the chamber can be calculated from the applied field strength (E) by using the formula for spherical somata

EQUATION 2

where *r* is the radius of the cell. Using the mean somal radius of our neurons (12 μm) as *r*, we calculated V_{membr} to be 0.3 V. This value is lower than the 0.5–1.5V required for electroporation with a single pulse (17), and is likely why we found that a single pulse was insufficient to electroporate neurons. However, we found that a 1 Hz train of five pulses reliably electroporated our cells.

Because significant Joule heating can occur during electroporation, we calculated the predicted temperature increase (Δ*T*) in the electroporation chamber following a single pulse, by using the conservative (over estimate) adiabatic equation:

EQUATION 3

where Δt is the pulse length, ρ is the density of the fluid, *c* is the heat capacity. Assuming that ρ and *c* of the saline are equal to those of water, ΔT is calculated to be 0.27K/pulse. Administration of five pulses, therefore, estimated to increase the temperature within the chamber by 1.4 K, is insufficient to cause neuronal injury by Joule heating.

Measurement of whole-cell capacitance

Bovine adrenal chromaffin cells were digested with collagenase and purified by density gradient centrifugation as described previously[18]. Cells were voltage-clamped in the whole-cell configuration (19). Electrodes were filled with (in millimolars): CsCl 110, MgCl2 4, HEPES 20, EGTA 10, GTP 0.35, ATP 4, and creatine phosphate 14, pH 7.3 (adjusted by CsOH); osmolality ≈ 310 mOsm. The extracellular recording medium contained (in millimolars): NaCl 130, glucose 20, Na-HEPES 10, $MgCl_2$ 1, KCl 2, and $CaCl_2$ 5, pH 7.3 with NaOH; osmolality ≈ 305 mOsm. Capacitance measurements were performed by using an Axopatch-1C patch-clamp amplifier and a computer-based phase tracking algorithm (20). To measure changes in capacitance, a 60 mV peak-to-peak sine wave (1.3 kHz) was added to the holding potential of –80 mV. The combination of sine wave and the holding potential was chosen (range of –110 to –50 mV) in order to provide a suitable signal-to-noise ratio without activating any voltage-dependent ion channels. The resulting current was analyzed at two orthogonal phase angles by using a software-based phase sensitive detector (PSD) with a temporal resolution of 10.24 ms per point (21). The phase-tracking technique allowed the determination of the correct phase angle for the PSD by switching a 500 kΩ resistor, in series with the cell input impedance and ground, in and out during sinusoidal stimulation. Conductance (series resistance) and capacitance values were continuously generated by the software. The deflections produced in the conductance plot by switching the resistor in and out serve as a 500 kΩ calibration for series resistance. Correct alignment of the PSD was achieved when these series resistance changes did not project into the capacitance plot. The whole-cell capacitance was canceled completely with the slow capacitance compensation. Unbalancing the slow capacitance compensation by 100 fF provided the calibration signal for capacitance trace.

The cell was perfused continually by Adams & List (Westbury, N.Y.) DAD-12 superfusion system after the formation of a whole-cell patch. In brief, this system consisted of a 'sewer pipe' arrangement in which quartz capillary of 100 μm diameter is placed close to cell. The sewer pipe was connected to six reservoirs, and flow from these was controlled by valves operated by AxoBasic (Foster City, Calif.) software. This arrangement enables the cell to be perfused continually with fresh solution and the rapid exchange of solutions for application of solutions containing PEG or P188. The exchange time for switch between two solutions was <1 s. The bath volume was kept relatively constant by using an outlet connected to a peristaltic pump. The capacitance difference before and after solution exchange was calibrated using a 100 fF calibration signal. Following washout of P188, the baseline was reset before conducting another trial.

Measurement of lipid peroxidation

Lipid peroxidation was measured using the oxidation-sensitive dye 4,4-difluoro-5-(4-phenyl-1, 3-butadienyl)-4-bora-3a,4a-diaza- s-indacene-3-undecanoic acid (C11-BODIPY$^{581/591}$). This

fatty acid does not fluoresce in aqueous solution. However, following partitioning into the plasma membrane (22), C11-BODIPY$^{581/591}$ is brightly fluorescent, is maximally excited at 581 nm, and emits (red) light at 591 nm. When exposed to oxidant stress, C11-BODIPY$^{581/591}$ is oxidized at a single diene bond (22). This oxidation alters its fluorescent properties so that C11-BODIPY$^{581/591}$ absorbs maximally at 488 nm and emits (green) light at 525 nm. Thus, the rate of change of green fluorescence in C11-BODIPY$^{581/591}$-loaded cells represents the rate of oxidation of membrane lipids.

Cultured neurons were exposed to C11-BODIPY$^{581/591}$ (1 μM) for 1 h at 37°C. During 40× microscopy and time-lapse imaging (see above), C11-BODIPY$^{581/591}$-containing neurons were excited with light from a 75w Xenon bulb attenuated by neutral density filters (ND 4) by using a 480 nm band pass filter, reflected by a polychroic mirror (51000, Chroma Technology) and the emitted light filtered by a 525 nm band pass filter. Regions of interest were identified, and mean somal fluorescence was measured. Lipid peroxidation was induced by Fenton reagent (23), by using Fe^{2+} and H_2O_2 to produce $OH^{\bullet}$: Following perfusion with HEPES-buffered saline, ferrous ammonium sulfate (200 nM) and H_2O_2 (100 μM) were added to the perfusate and changes in oxidized C11-BODIPY$^{581/591}$ fluorescence monitored. After 10–15 min, P188 (100 μM) was added to the Fenton reagent and fluorescence monitoring continued. Changes in oxidized C11-BODIPY$^{581/591}$ fluorescence expressed in terms of percentage change from baseline values; baseline value for each cell was defined as the mean of the five baseline values immediately preceding perfusions of Fenton reagent. Data were plotted on a cell-by-cell basis as a function of time. For each cell, the rate of rise of oxidized C11-BODIPY$^{581/591}$ fluorescence during Fenton reagent and Fenton reagent plus Poloxamer 188 were calculated. Tests of significance were by ANOVA for repeated measures.

Materials

Poloxamer 188 was a gift from BASF AG (Gurnee, Ill.). Cultures of fetal rat cerebellar Purkinje neurons were a kind gift of J. Brorson. Calcein-AM, propidium iodide, fura-4F-AM and C11-Bodipy$^{581/581}$ were obtained from Molecular Probes (Eugene, Ore.). NMDA and kainate were obtained from Research Biochemical (Natick, Mass.). Platinum electrodes and all other chemicals were obtained from Sigma (St. Louis, Mo.).

RESULTS

Poloxamer protects neurons following necrotic injury

We hypothesized that P188 protects neurons *in vitro* from stimuli in which necrosis and loss of membrane integrity contribute to neuronal death. In addition, we hypothesized that P188 would not protect neurons from apoptosis-inducing stimuli, where nuclear and cytoplasmic condensation occur without breach of the cell membrane (24). We used embryonic rat hippocampal neurons to assess the effect of P188 on neuronal survival following intense NMDA receptor stimulation, a model of hippocampal neuronal death in which necrosis plays a prominent role (7). Neurons were briefly incubated in NMDA or vehicle, and survival quantified 48 h later. Incubation of neurons in vehicle alone resulted in 71.05% ± 1.04 (SE) neuronal survival at 48 h, and incubation in NMDA (300 μM) significantly reduced survival at 48 h to 33.8% ±0.80 (SE). Remarkably, P188 (100 μM), added to the culture medium into which neurons were placed following NMDA, provided complete neuroprotection at 48 h against the actions of NMDA (**Fig. 2a**). Specifically, addition of P188 to the culture medium following incubation in NMDA significantly increased 48-h survival at to 73.3% ±0.66 (SE; $p<0.0001$; N=12,325 cells on 12 coverslips), slightly greater than vehicle alone, reducing NMDA-induced mortality to zero.

We next tested whether P188 improved neuronal survival following other insults resulting in loss of membrane integrity. We measured P188-induced neuroprotection at 48 h of cerebellar Purkinje neurons following 15-min incubations in kainate (100 μM), as well as of hippocampal neurons at 48 h following 15-min incubations in menadione (30 μM) or tert-butyl-hydroperoxide (t-BuOOH, 100 μM). We also measured P188 neuroprotection at 48 h following a 15-min incubation in staurosporine (200 μM), an insult after which the plasma membrane remains intact.

In all cultures, neuronal survival at 48 h following exposure to vehicle alone was >70% (**Fig. 2b**). Following toxin exposure, 48 h-survival fell to 30%–50%, depending on toxin (**Fig. 2b**). P188 significantly increased survival following kainate, menadione, and t-BuOOH exposure (**Fig. 2b**): survival approached control levels ($p<0.001$ for each toxin, N=6 coverslips per condition per toxin). In contrast, P188 increased 48 h survival following staurosporine only slightly (27.59 ± 1.3% SE staurosporine *vs.* 37.75 ± 2.08% staurosporine followed by P188 SE; **Fig. 2b**). This increase, although statistically significant ($p<.01$), was far less than the neuroprotection seen in the other models studied. These results indicate that P188 markedly increases neuronal survival following insults in which necrosis plays a prominent role, but fails to provide similar protection from apoptosis.

Characteristics of P188 neuroprotection following NMDA-induced injury

We next investigated the dose- and time-dependence of P188-induced neuroprotection following intense NMDA stimulation. When neurons were placed into culture media containing P188 immediately following NMDA exposure, survival at 48 h post-NMDA significantly depended on P188 concentration ($p<0.001$, N=6 coverslips per condition, **Fig. 2c**). The concentration-survival relationship was U-shaped, with maximum survival occurring at $10^{-4.5}$ M. Above this concentration, survival progressively declined, as P188 concentration approached the critical micellar concentration (6.3 mM at 37°C) (25). Survival at 48 h decreased progressively with increasing delay of administration after NMDA ($p<0.001$, N=6 coverslips per condition), with the efficacy of neuronal rescue lowest at 4 h post-injury onset, but still 120% of survival following NMDA alone. Survival increased when P188 was administered 8 h following NMDA (55.3 ± 4.0% (SE) *vs.* 22.5 ± 1.8% (SE) control, **Fig. 2D**).

Poloxamer 188 does not block NMDA receptors or alter increases in $[Ca^{2+}]_i$

Reduction of NMDA current by P188-mediated antagonism of NMDA receptors could contribute to the broad, P188-induced neuroprotection, both directly and via blockade of excitatory neurotransmission (26). Accordingly, we made whole-cell patch clamp recordings of NMDA-induced currents in embryonic hippocampal neurons, in the absence and presence of P188 (100 μM). Peak NMDA-induced inward currents in the presence and absence of P188 were not significantly different (control 390 ± 49 pA, P188 356 ± 38 pA, N=5; p=0.5, **Fig. 3a**). We also measured NMDA effects on $[Ca^{2+}]_i$ in the absence and presence of P188 (100 μM), using the low-affinity Ca^{2+} reporter, Fura-4F (Kd for Ca^{2+} 700 nM). Mean peak somal $[Ca^{2+}]_i$ during a 10-s exposure to NMDA (300 μM) did not differ significantly between the presence or absence of P188 (control 327 ± 30 nM *vs.* P188 384 ± 37 nM, N=13, **Fig. 3b**).

Our measurements of neuronal survival used a live-dead cell assay, which provided no information regarding whether P188 preserved membrane receptor or intracellular functions specific to neurons. Accordingly, we performed time-lapse imaging studies of $[Ca^{2+}]_i$ responses to membrane depolarization and NMDA receptor stimulation at 48 h and at 5 d following NMDA. Neurons exposed to intense NMDA receptor stimulation followed by 48-h incubation in culture media containing P188 produced a homogenous population of neurons (18/18 neurons studied on six coverslips) whose mean somal $[Ca^{2+}]_i$ at baseline (N=18) was no different from baseline $[Ca^{2+}]_i$ of neurons not exposed to NMDA (70.6 ± 4.3 nM, SE). Brief (20 s) depolarization with 60 mM KCl abruptly increased mean somal $[Ca^{2+}]_i$ to 675 ± 119 nM (SE). Similarly, 20-s stimulation with NMDA (300 μM) increased mean somal $[Ca^{2+}]_i$ to 534 ± 99 nM (SE). Following removal of each stimulus, $[Ca^{2+}]_i$ returned rapidly to baseline values (**Fig. 2e**). The results indicate that, following P188-mediated rescue of neurons from NMDA injury: 1) $[Ca^{2+}]_i$ homeostatic mechanisms are intact; 2) voltage-gated Ca^{2+} channels and NMDA receptor coupled Ca^{2+} channels function normally; 3) following an intracellular Ca^{2+} load, $[Ca^{2+}]_i$ is appropriately decreased to baseline values.

The absence of significant effects of P188 on either NMDA receptor-mediated inward currents or the magnitude of NMDA-induced [Ca2+]i increases indicate that P188 protects neurons from injury by mechanisms unrelated to NMDA receptor activation or subsequent $[Ca^{2+}]_i$ elevation.

Poloxamer inserts into the plasma membrane

Having excluded potential P188 effects on NMDA receptor activation and $[Ca^{2+}]_i$ increases, we determined the cellular sites at which P188 exerts its neuroprotective effects. P188 inserts itself into lipid bilayers (11), and we hypothesized that insertion occurred into the plasma membrane of living cells. We obtained evidence of insertion of P188 into the plasma membrane of intact cells by measuring P188-induced changes in cell surface area. To measure these changes, we used continuous measurements of whole-cell capacitance in bovine adrenal chromaffin cells.

Mean capacitance of chromaffin cells before P188 perfusion was 5.1±0.28 pF (SE, n=8). Perfusion of P188 (100 μM) increased cell capacitance in all cells for the duration of the perfusion (40 s). Capacitance initially increased in a rapid, step-like fashion, followed by a steady, linear increase during the 40-s perfusion (**Fig. 4a**). With removal of P188, capacitance decreased over the subsequent 40 s to approximately 15 fF above baseline. Mean peak capacitance increase was 54 fF ± 7.8 (SE, n=8). Repetitive P188 applications increased capacitance above baseline, but with a smaller rise with each successive application (**Fig. 4b**).

Eighty percent of the P188 molecule consists of poly(ethylene glycol) polymers (PEGs). PEGs, lower the activity of water adjacent to the membrane, forcing very close contact between vesicle membranes (27). We determined the extent to which the P188-induced capacitance changes were due to interactions of the PEO blocks with the surface of the cell membrane, rather than insertion into the membrane, by measuring whole-cell capacitance changes during perfusion of a PEG of similar molecular weight (8, 400). PEG (100 μM) perfusion did transiently increase whole-cell capacitance above baseline values (32.8 fF ± 8.7 PEG), but significantly less than P188 (**Fig. 4a**). In contrast to P188, removal of PEG from the perfusate caused the capacitance to decrease to baseline. Furthermore, repeated perfusion with PEG increased capacitance by the same amount each time (**Fig. 4b**). This fixed, completely reversible PEG-induced capacitance increase contrasted markedly with that observed following P188.

Poloxamer 188 restores disruption of membrane integrity

Our finding of P188 insertion into the neuronal plasma membrane suggested that P188 restores neuronal membrane integrity, similar to nonneuronal cells (8–10). To assess P188 restoration of membrane integrity, we directly disrupted neuronal membranes by using electroporation. We used electroporation because it is a reasonably well-understood method of membrane disruption that can be induced independent of receptor activation, signal transduction, or intracellular mechanisms. Significant restoration of membrane integrity by P188 following membrane electroporation would demonstrate a direct action of P188 on the cell membrane.

Neurons were loaded with calcein, a membrane-impermeant dye with primarily cytosolic distribution, and time-lapse microfluorimetry was performed of intracellular fluorescence before, during, and after electroporation. A single, brief train (1-s duration, 5 Hz) of current pulses caused rapid and complete loss of intracellular fluorescence across all cells within the field-of-view of the camera (0.04 mm^2) over 30–60 s (n=10 trials, 25–50 cells per trial). In contrast, perfusion of P188 (30 μM) onto neurons following electroporation reliably arrested dye loss (**Fig. 5**). We typically observed variable degrees of fluorescence loss between cells within a single field prior to arrest of dye loss. However, in experiments in which P188 perfusion was initiated within 20 s following shocks, intracellular fluorescence of all cells stabilized after application of P188. Applying P188 in more than about 20 s following shocks did not reliably decrease the rate of dye loss.

Poloxamer 188 blocks plasma membrane peroxidation

Lipid peroxides can be formed by activation of glutamate receptors (28), with subsequent production of reactive oxygen species (6) leading to membrane damage. The presence of P188 in the plasma membrane suggests that P188 may reduce lipid peroxidation from reactive oxygen species. To test this hypothesis, we assessed the effect of P188 on the rate of induced lipid peroxidation in single, living hippocampal neurons. We induced lipid peroxidation via the Fenton reaction, perfusing neurons with $Fe(NH_4)_2(SO_4)_2$ (200 μM) and H_2O_2 (1 mM). To measure lipid peroxidation, we performed time-lapse imaging of neurons loaded with C11-BODIPY$^{581/591}$, an oxidation-sensitive lipid, and monitored the increase of oxidation-dependent fluorescence.

Perfusing neurons with HEPES-buffered saline in the absence of Fe^{2+} and H_2O_2 produced stable oxidized C11-BODIPY$^{581/591}$ fluorescence. Addition of Fe^{2+} and H_2O_2 to neurons was followed by a steady increase in fluorescence that continued until the Fe^{2+} and H_2O_2 were removed (**Fig. 6**). However, adding P188 (30 μM) to the perfusate during Fe^{2+} and H_2O_2 administration abruptly and consistently decreased the rate of fluorescence increase (1.49 ± 0.48 %/min Fe^{2+} plus H_2O_2 alone *vs.* 0.64 ± 0.14%/min P188 plus Fe^{2+} plus H_2O_2, n=16 neurons in four trials; $p<0.001$; **Fig. 6**). Furthermore, addition of Fe^{2+} and H_2O_2 to neurons perfused with P188 prevented increased in oxidized C11-BODIPY$^{581/591}$ fluorescence. These observations show that P188 significantly inhibits the rate of lipid peroxidation in the presence of continuous oxidative stimulation.

DISCUSSION

This report is the first to demonstrate that an amphiphilic, tri-block copolymer, Poloxamer 188, provides robust neuroprotection *in vitro* following intense excitotoxicity or oxidative stress—insults resulting in loss of membrane integrity (7). Five days after injury, neurons rescued by P188 demonstrate intact function of intracellular enzymes, cell surface receptors, voltage-gated channels, and $[Ca^{2+}]_i$ homeostasis. In addition, P188-induced neuroprotection still occurs when a significant delay (8 h) elapses between insult and P188 administration. It is unclear whether the increased neuronal survival, observed with P188 administration 8 h post-NMDA, occurs because P188 is present during an period when mechanisms of delayed death, for example, superoxide production (29), are particularly important.

The importance of neuronal necrosis following intense excitotoxicity and oxidative stress from many causes (30–32) demonstrates the potential of Poloxamer 188, and of amphiphilic, tri-block copolymer surfactants in general, in protecting neurons from important mechanisms of brain injury. The use of these molecules, therefore, represents a novel therapy for brain injuries in which these mechanisms play a central role.

In contrast to its effect on neurons following stimuli-inducing necrosis, P188 did not protect neurons from staurosporine-induced apoptotic death well. Apoptotic death is characterized by preservation of membrane integrity (24). This relative absence of neuroprotection is consistent with the mechanisms of P188-induced neuroprotection that we have observed, namely blocking and repairing damage to the plasma membrane.

P188 did not alter NMDA receptor currents, demonstrating absence of a significant P188 effect on NMDA receptor function. Similarly, the absence of a smaller amplitude or a shorter duration $[Ca^{2+}]_i$ response during P188 treatment demonstrates that P188 does not alter either voltage-gated Ca^{2+} channels or NMDA receptor-mediated Ca^{2+} influx. We used Fura-4F (KD 700 nM), because low-affinity reporters distinguish toxic $[Ca^{2+}]_i$ responses from nontoxic responses (33)and high-affinity Ca^{2+} indicators do not (34). These data, however, do not exclude a presynaptic effect of P188 on transmitter release.

P188 markedly increased whole-cell capacitance, demonstrating that P188 increased cell surface area. This cell surface area increase constitutes indirect evidence that P188 inserts into the plasma membrane. This evidence is consistent with theoretical predictions of P188 behavior from its amphiphilic, tri-block structure, and from observations of P188 insertion into lipid bilayers (11). However, the precise nature of the interaction between P188 and cell membranes is not apparent from these data.

It is unlikely that the P188-induced capacitance increase is due to the same mechanisms causing the small, PEG-induced increase. First, each PEO block (3500 mw) is <50% of the size of PEG, yet the capacitance increase was 150% of that seen with PEG. Second, we observed markedly different patterns of capacitance increase upon repeated application in the same cell: The magnitude of the P188-induced capacitance rise decreased progressively with repeated application, whereas that of PEG was stable. The much smaller capacitance increases we observed with similarly sized PEG may be due to a combination of alterations in local membrane permittivity (dipole density), and dehydration-induced decreases in membrane thickness.

Insertion of P188 into the membrane provides an attractive mechanism for the P188-induced restoration of membrane integrity, which we observed following electroporation. Electropores typically remain in the membrane for minutes (35); with sufficient pore density, loss of intracellular contents will result. In our system, five shocks produced complete loss of intracellular fluorescence within 1 min, and this loss was arrested by P188 application. Tri-block copolymers seal membranes following electroporation of other cell types (9, 36) and following Joule heating-induced loss of membrane integrity (13). Similarly, application of PEG to the site of severe compression injury of the spinal cord has been followed by immediate recovery of nerve conduction (37), apparently due to membrane sealing. Our finding that P188 significantly reduces neuronal membrane permeability following electroporation also indicates that P188 preserves neuronal function following physical damage to the membrane. Tri-block amphiphilic copolymers may, therefore, have significant clinical application in the therapy of brain injury following electrical trauma.

Loss of membrane integrity also occurs following excitotoxic or oxidative stimulation (7), through multiple mechanisms, including swelling and membrane peroxidation. The marked swelling of soma and dendrites that can accompany severe

excitotoxic injury (38) may progress to frank membrane rupture and loss of intracellular contents (39). P188-induced membrane sealing may contribute to the reduction of neuronal death we observed by preventing or restoring early loss of membrane integrity in susceptible neurons.

In addition to its direct effects on membrane integrity, P188 almost completely blocked lipid peroxidation induced by Fe^{2+} and H_2O_2. NMDA-induced increases in free radical production (40) and subsequent lipid peroxidation (41), as well as antioxidant-induced neuroprotection following NMDA (42) demonstrate that reactive oxygen species play a central role in excitotoxic neuronal death. Increased superoxide levels 4–8 h after NMDA stimulation (29) and the finding of 4-hydroxyalkenal products of lipid peroxide decomposition 24 h following kainate (43) indicate that superoxide-induced lipid peroxidation likely occurs during the same period that we observed P188 neuroprotection. Whether oxidation or other radical transformation of P188 occurs following NMDA is unknown, and it is also possible that P188 reduces lipid peroxidation by scavenging reactive oxygen species directly. In any case, blockade of lipid peroxidation may underlie a portion of P188-induced neuroprotection.

Blockade of lipid peroxidation underlies the marked neuroprotection observed with malonic acid derivatives of buckminsterfullerenes (44) following NMDA. These derivatives avidly trap free radicals (44), and the increased neuroprotection seen with more amphiphilic derivatives has been ascribed to the greater penetration of the carbon sphere into the membrane (44). Our indirect evidence of P188 insertion into the membrane is consistent with the hypothesis that its profound reduction in lipid peroxidation is mediated by the hydrophobic polypropylene block. If membrane insertion does underlie this peroxidation reduction, the 80% hydrophilic PEO content of P188 would be advantageous; such hydrophilicity confers upon the molecule high aqueous solubility, so that the hypothesized membrane penetration is not offset by reduced H_2O solubility.

The present study demonstrates that an amphiphilic tri-block copolymer provides profound protection *in vitro* against a variety of stimuli resulting in neuronal necrosis. Although the differences in the experimental conditions we used to investigate each mechanism in isolation do not allow synthesis of a coherent mechanism of P188-induced neuroprotection, we have demonstrated that P188 blocks discrete, well-described mechanisms known to play roles in NMDA-induced neuronal injury. The hypothesized role of P188 in blocking these mechanisms following NMDA receptor stimulation is summarized in Figure 7.

Many current approaches to neuroprotection, including antagonism of ligand- and voltage-gated ionic mechanisms of neuronal injury, have proven largely ineffective in clinical settings (45). Because the mechanisms of action are specifically directed at the plasma membrane, use of amphiphilic, tri-block copolymers may provide an alternate therapeutic approach to neuronal necrosis.

ACKNOWLEDGMENTS

We thank Vytas Bindokas for a critical reading of the manuscript, and Jurgen Hannig, and Ka Yee Lee for their helpful discussions. We also thank Xiao-min Zhang for expert technical assistance. Supported in part by National Institutes of Health grants GM53113 and EPRI RPWO2914.

REFERENCES

1. Choi, D. W. (1988) Glutamate neurotoxicity and disease of the central nervous system. *Neuron* 1, 623–634
2. Choi, D. W. (1987) Ionic dependence of glutamate neurotoxicity. *J. Neurosci.* **7,** 369–379
3. Nicholls, D. G. and Budd, S. L. (2000) Mitochondria and Neuronal Survival. *Phys. Rev.* **80,** 316–360
4. Dawson, V., Kizushi, V., Huang, P., Snyder, S., and Dawson, T. (1996) Resistance to neurotoxicity in cortical cultures from neuronal nitric oxide synthase-deficient mice. *J. Neurosci.* **16(8),** 2479–2487
5. Patel, M., Day, B. J., Crapo, J. D., Fridovich, I., and McNamara, J. O. (1996) Requirement for superoxide in excitotoxic cell death. *Neuron* **16,** 345–355
6. Murphy, M. P., Packer, M. A., Scarlett, J. L., and Martin, S. W. (1998) Peroxynitrite: a biologically significant oxidant. *Gen. Pharmacol.* **31,** 179–186
7. Bonfoco, E., Krainc, D., Ankarcrona, M., Nicotera, P., and Lipton, S. A. (1995) Apoptosis and necrosis: two distinct events induced, respectively, by mild and intense insults with N-methyl-D-aspartate or nitric oxide/superoxide in cortical cell cultures. *Proc. Natl. Acad. Sci. US A* **92,** 7162–7166
8. Bischof, J. C., Padanilam, J., Holmes, W. H., Ezzell, R. M., Lee, R. C., Tompkins, R. G., Yarmush, M. L., and Toner, M. (1995) Dynamics of cell membrane permeability changes at supraphysiological temperatures. *Biophys. J.* **68,** 2608–2614
9. Lee, R. C., Canaday, D. J., and Hammer, S. M. (1993) Transient and stable ionic permeabilization of isolated skeletal muscle cells after electrical shock. *J. Burn Care Rehabil.* **14,** 528–540
10. Hannig, J., Yu, J., Beckett, M., Weichselbaum, R., and Lee, R. C. (1999) Poloxamine 1107 sealing of radiopermeabilized erythrocyte membranes. *Int. J. Radiat. Biol.* **75,** 379–385
11. Baekmark, T. R., Pedersen, S., Jorgensen, K., and Mouritsen, O. G. (1997) The effects of ethylene oxide containing lipopolymers and tri-block copolymers on lipid bilayers of dipalmitoylphosphatidylcholine. *Biophys. J.* **73,** 1479–1491
12. Lee, R. C., River, L. P., Pan, F. S., Ji, L., and Wollmann, R. L. (1992) Surfactant-induced sealing of electropermeabilized skeletal muscle membranes *in vivo*. *Proc. Natl. Acad. Sci. USA* **89,** 4524–4528
13. Merchant, F. A., Holmes, W. H., Capelli-Schellpfeffer, M., Lee, R. C., and Toner, M. (1998) Poloxamer 188 enhances functional recovery of lethally heat-shocked fibroblasts. *J. Surg. Res.* **74,** 131–140
14. Banker, G. A. and Cowan, W. M. (1977) Rat hippocampal neurons in dispersed cell culture. *Brain Res.* **126,** 397–342
15. Scheffe, H. (1953) A method for judging all contrasts in the analysis of variance. *Biometrika* **40,** 87–104
16. Chemical Rubber Company (1999) *CRC Handbook of Chemistry and Physics*. Chapman and Hall: Boca Raton, FL
17. Weaver, J. C. (1993) Electroporation: a general phenomenon for manipulating cells and tissues. *J. Cell. Biochem.* **51,** 426–435
18. Artalejo, C. R., Rossie, S., Perlman, R. L., and Fox, A. P. (1992) Voltage-dependent phosphorylation may recruit Ca2+ current facilitation in chromaffin cells. *Nature* (*London*) **358,** 63–66
19. Hamill, O. P., Marty, A., Neher, E., Sakmann, B., and Sigworth, F. J. (1981) Improved patch-clamp techniques for high-resolution current recording from cells and cell-free membrane patches. *Pflugers Arch.* **391,** 85–100

20. Fidler, N. and Fernandez, J. M. (1989) Phase tracking: an improved phase detection technique for cell membrane capacitance measurements. *Biophys. J.* **56,** 1153–1162
21. Joshi, C., and Fernandez, J. M. (1988) Capacitance measurements. An analysis of the phase detector technique used to study exocytosis and endocytosis. *Biophys. J.* **53,** 885–892
22. Pap, E. H., Drummen, G. P., Winter, V. J., Kooij, T. W., Rijken, P., Wirtz, K. W., Op den Kamp, J. A., Hage, W. J., and Post, J. A. (1999) Ratio-fluorescence microscopy of lipid oxidation in living cells using C11-BODIPY(581/591). *FEBS Lett.* **453,** 278–282
23. Winterbourn, C. C. (1995) Toxicity of iron and hydrogen peroxide: the Fenton reaction. *Toxicol. Lett.* **82-83,** 969–974
24. Colbourne, F., Sutherland, G. R., and Auer, R. N. (1999) Electron microscopic evidence against apoptosis as the mechanism of neuronal death in global ischemia. *J. Neurosci.* **19,** 4200–4210
25. Kabanov, A., Nazarova, I., Astafieva, I., Batrakova, E., Alakhov, V., Yaroslavov, A., and Kabanov, V. (1995) Micelle formation and solubilization of fluorescent probes in poly(oxyethylene-b-oxypropylene) solutions. *Macromolecules* **28,** 2303–2314
26. Abele, A. E., Scholz, K. P., Scholz, W. K., and Miller, R. J. (1990) Excitotoxicity induced by enhanced excitatory neurotransmission in cultured hippocampal pyramidal neurons. *Neuron* **4,** 413–419
27. Burgess, S. W., McIntosh, T. J., and Lentz, B. R. (1992) Modulation of poly(ethylene glycol)-induced fusion by membrane hydration: importance of interbilayer separation. *Biochemistry* **31,** 2653–2661
28. Monyer, H., Hartley, D. M., and Choi, D. W. (1990) 21-Aminosteroids attenuate excitotoxic neuronal injury in cortical cell cultures. *Neuron* **5,** 121–126
29. Luetjens, C. M., Bui, N. T., Sengpiel, B., Munstermann, G., Poppe, M., Krohn, A. J., Bauerbach, E., Krieglstein, J., and Prehn, J. H. (2000) Delayed mitochondrial dysfunction in excitotoxic neuron death: cytochrome *c* release and a secondary increase in superoxide production. *J. Neurosci.* **20,** 5715–5723
30. Kondo, T., Reaume, A. G., Huang, T. T., Carlson, E., Murakami, K., Chen, S. F., Hoffman, E. K., Scott, R. W., Epstein, C. J., and Chan, P. H. (1997) Reduction of CuZn-superoxide dismutase activity exacerbates neuronal cell injury and edema formation after transient focal cerebral ischemia. *J. Neurosci.* **17,** 4180–4189
31. McIntosh, T. K., Saatman, K. E., Raghupathi, R., Graham, D. I., Smith, D. H., Lee, V. M., and Trojanowski, J. Q. (1998) The Dorothy Russell Memorial Lecture. The molecular and cellular sequelae of experimental traumatic brain injury: pathogenetic mechanisms. *Neuropathol. Appl. Neurobiol.* **24,** 251–267
32. Guo, Q., Sopher, B. L., Furukawa, K., Pham, D. G., Robinson, N., Martin, G. M., and Mattson, M. P. (1997) Alzheimer's presenilin mutation sensitizes neural cells to apoptosis induced by trophic factor withdrawal and amyloid beta-peptide: involvement of calcium and oxyradicals. *J. Neurosci.* **17,** 4212–4222
33. Hyrc, K., Handran, S. D., Rothman, S. M., and Goldberg, M. P. (1997) Ionized intracellular calcium concentration predicts excitotoxic neuronal death: observations with low-affinity fluorescent calcium indicators. *J. Neurosci.* **17,** 6669–6677
34. Sattler, R., Charlton, M. P., Hafner, M., and Tymianski, M. (1998) Distinct influx pathways, not calcium load, determine neuronal vulnerability to calcium neurotoxicity. *J. Neurochem.* **71,** 2349–2364
35. DeBruin, K. A., and Krassowska, W. (1999) Modeling electroporation in a single cell. I. Effects of field strength and rest potential. *Biophys. J.* **77,** 1213–1224
36. Bier, M., Hammer, S. M., Canaday, D. J., and Lee, R. C. (1999) Kinetics of sealing for transient electropores in isolated mammalian skeletal muscle cells. *Bioelectromagnetics* **20,** 194–201
37. Borgens, R. B. and Shi, R. (2000) Immediate recovery from spinal cord injury through molecular repair of nerve membranes with polyethylene glycol. *FASEB J.* **14,** 27–35
38. Bindokas, V. P. and Miller, R. J. (1995) Excitotoxic degeneration is initiated at non-random sites in cultured rat cerebellar neurons. *J. Neurosci.* **15,** 6999–7011
39. Marks, J. D., Friedman, J. E., and Haddad, G. G. (1996) Vulnerability of CA1 neurons to glutamate is developmentally regulated. *Brain Res. Dev. Brain Res.* **97,** 194–206
40. Reynolds, I. J. and Hastings, T. G. (1995) Glutamate induces the production of reactive oxygen species in cultured forebrain neurons following NMDA receptor activation. *J. Neurosci.* **15,** 3318–3327
41. Farooqui, A. A., and Horrocks, L. A. (1998) Lipid peroxides in the free radical pathophysiology of brain diseases. *Cell Mol. Neurobiol.* **18,** 599–608
42. Yue, T. L., Gu, J. L., Lysko, P. G., Cheng, H. Y., Barone, F. C., and Feuerstein, G. (1992) Neuroprotective effects of phenyl-t-butyl-nitrone in gerbil global brain ischemia and in cultured rat cerebellar neurons. *Brain Res.* **574,** 193–197
43. Ong, W., Lu, X., Hu, C., and Halliwell, B. (2000) Distribution of hydroxynonenal-modified proteins in the kainate- lesioned rat hippocampus: evidence that hydroxynonenal formation precedes neuronal cell death [In Process Citation]. *Free Radic. Biol. Med.* **28,** 1214–1221
44. Dugan, L. L., Turetsky, D. M., Du, C., Lobner, D., Wheeler, M., Almli, C. R., Shen, C. K., Luh, T. Y., Choi, D. W., and Lin, T. S. (1997) Carboxyfullerenes as neuroprotective agents [published erratum appears in *Proc. Natl. Acad. Sci. USA* (1997) Oct. 28; **94(22),**12241]. *Proc. Natl. Acad. Sci. USA* **94,** 9434–9439
45. Lee, J. M., Zipfel, G. J., and Choi, D. W. (1999) The changing landscape of ischaemic brain injury mechanisms. *Nature* (*London*) **399,** A7–A14

Received September 20, 2000; revised November 27, 2000.

Equation 1

$$J = \sigma \cdot E$$

Equation 2

$$V_{membr} = \frac{3}{2} r \cdot E$$

Equation 3

$$\frac{\Delta T}{\Delta t} = \rho \cdot c \cdot E^2$$

Fig. 1

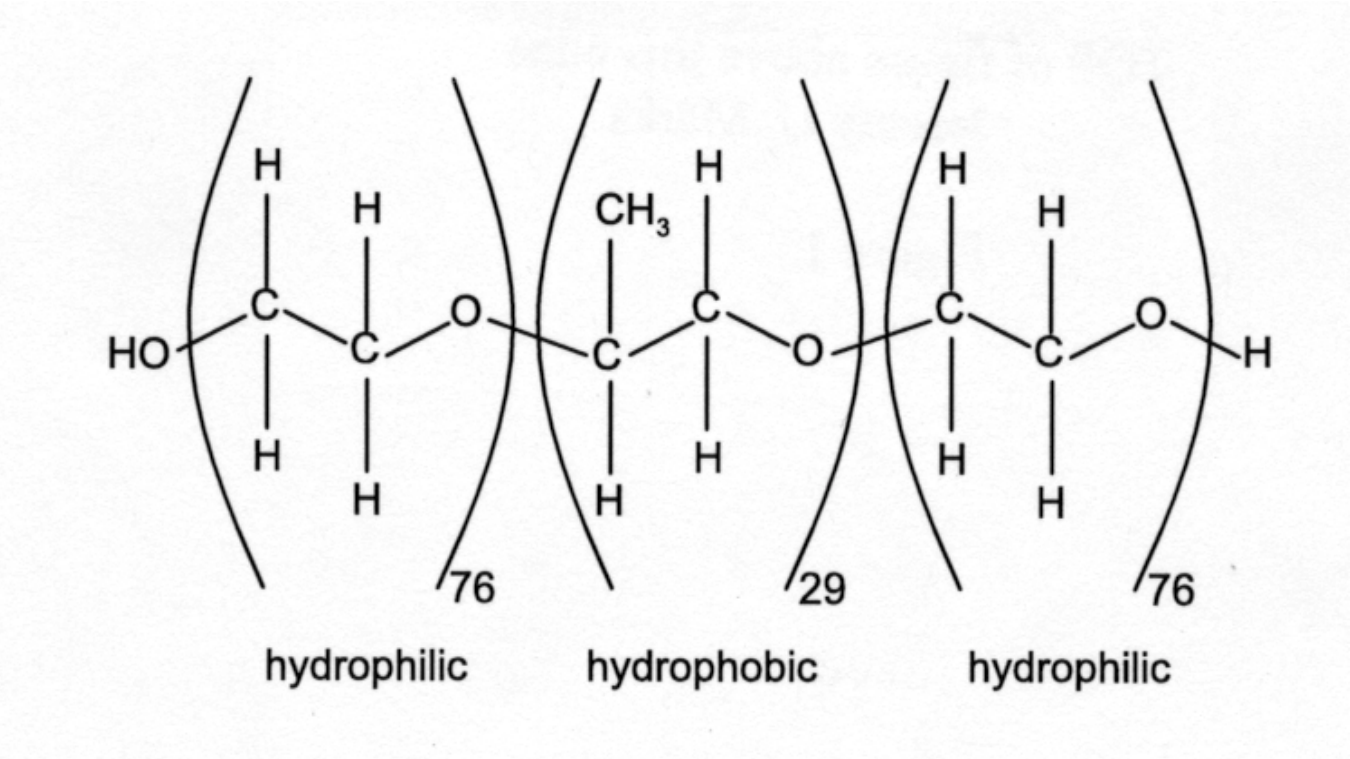

Figure 1. Structure of Poloxamer 188.

Fig. 2

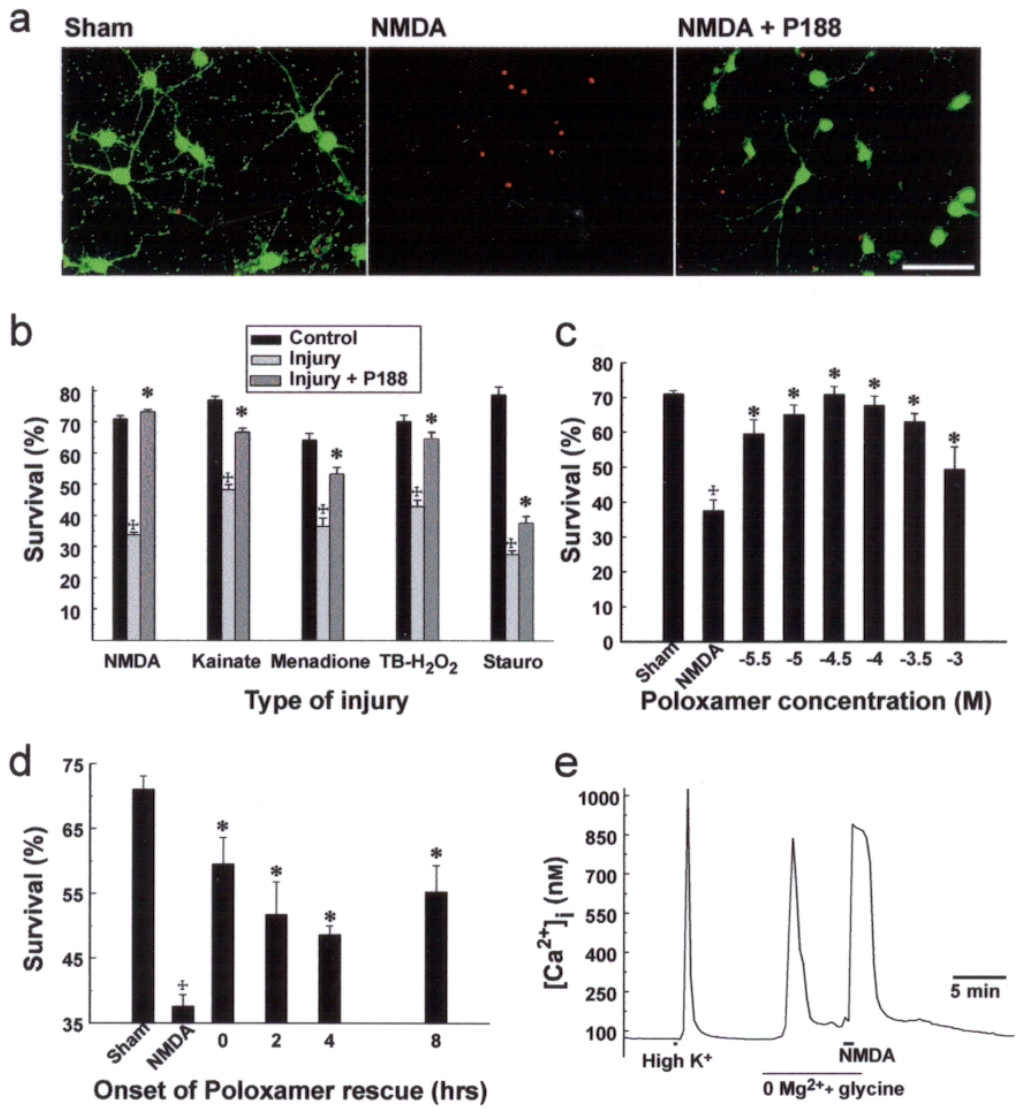

Figure 2. Poloxamer 188 protects neurons from stimuli-inducing necrosis *in vitro*. (a) Representative fields of hippocampal neurons 48 h following 15-min exposure to buffer (left), NMDA (300 μm) alone (center), or NMDA followed by P188 (100 μM) in the culture media (right). Living neurons are stained with calcein (green), and dead neurons have nuclei stained with propidium iodide (red). **(b)** Neuronal survival 48 h following intense excitotoxic (NMDA, kainate) and oxidative (menadione, *tert*-butyl-hydroperoxide) insults resulting in necrosis and staurosporine. Hippocampal neurons were used for all stimuli except kainate (100 μM), when cultured embryonic cerebellar Purkinje neurons were used. Bars represent sum of six coverslips per condition per toxin. Error bars are SE. Statistical significance between groups (crosses, toxin treatment vs. control; asterisks, toxin with P188 vs. toxin alone) determined with the likelihood ratio test (with correction for multiple comparisons) following overall significance by logistic regression. **(c)** Survival of hippocampal neurons following NMDA (300 μM) and different concentrations of P188. Bars represent sum of six coverslips per condition per P188 concentration, and error bars represent the standard error of the mean. Sham represents 15-min incubation in HEPES-buffered saline. Statistical significance between groups (crosses, toxin treatment vs. control; asterisks, toxin with P188 vs. toxin alone) determined as in (b) above. **(d)** Survival of hippocampal neurons following NMDA and increasing delays between NMDA and addition of P188 to the cultures. Purkinje neurons were used. Bars represent sum of six coverslips per condition per toxin. Error bars are SE. Statistical significance between groups (crosses, toxin treatment vs. control; asterisks, toxin with P188 vs. toxin alone) determined as in (b) above. **(e)** Changes in $[Ca^{2+}]_i$, reported by Fura-2, of a single hippocampal neuron 5 days after exposure to NMDA (300 μm). Following NMDA, P188 (30 μM) was added to the culture medium. High K represents exposure to KCl (60 mM). NMDA (2nd bar) is 300 μm.

Fig. 3

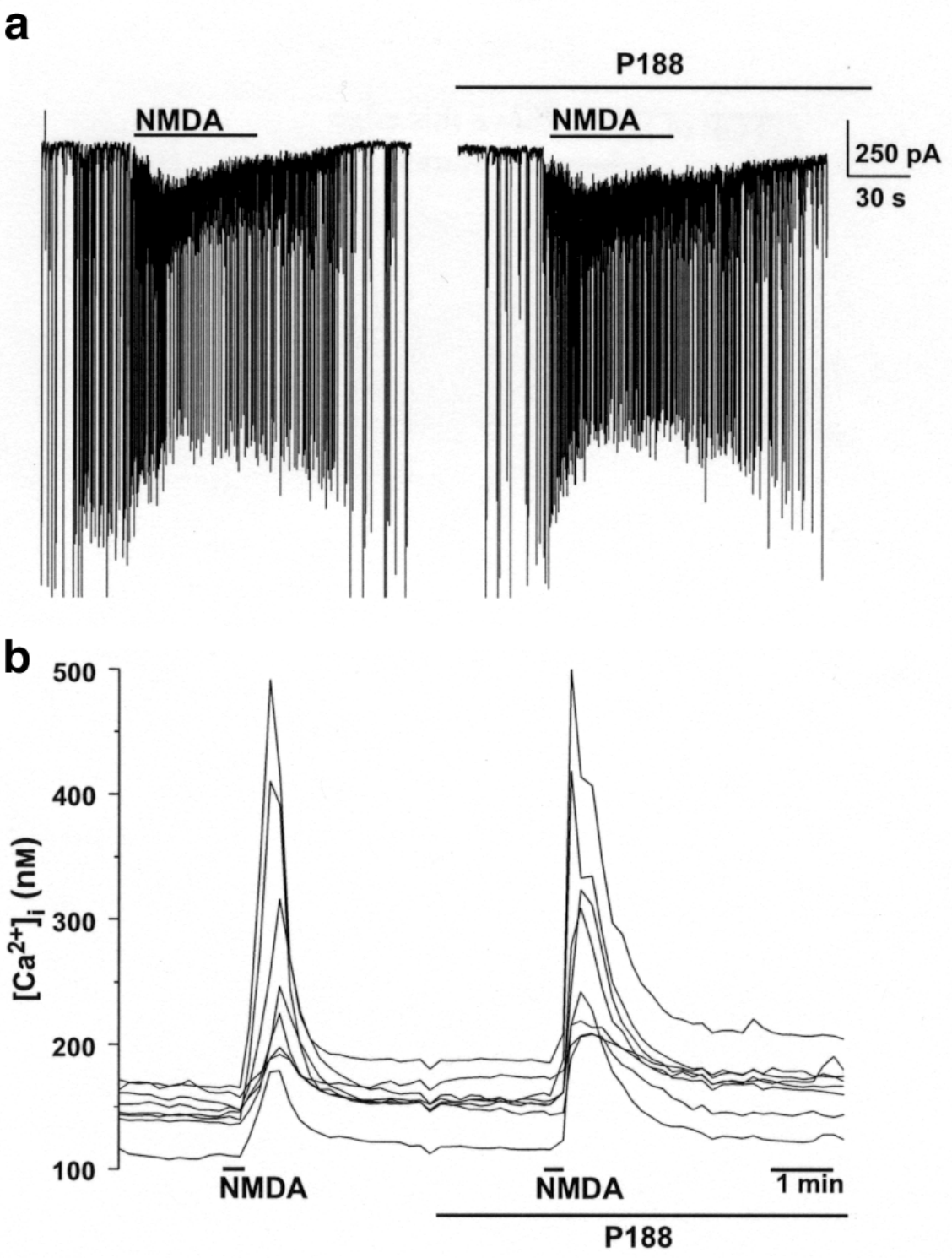

Figure 3. P188 does not alter NMDA currents or the magnitude of NMDA -induced $[Ca^{2+}]_i$ increase. (a) Voltage record of a single hippocampal neuron during brief perfusion with NMDA (100 μM) and NMDA in the presence of P188 (100 μM). **(b)** Superimposed $[Ca^{2+}]_i$ responses, reported by Fura-4F (Kd 700 nM), of hippocampal neurons to NMDA (300 μM) and NMDA in the presence of P188 (100 μM).

Fig. 4

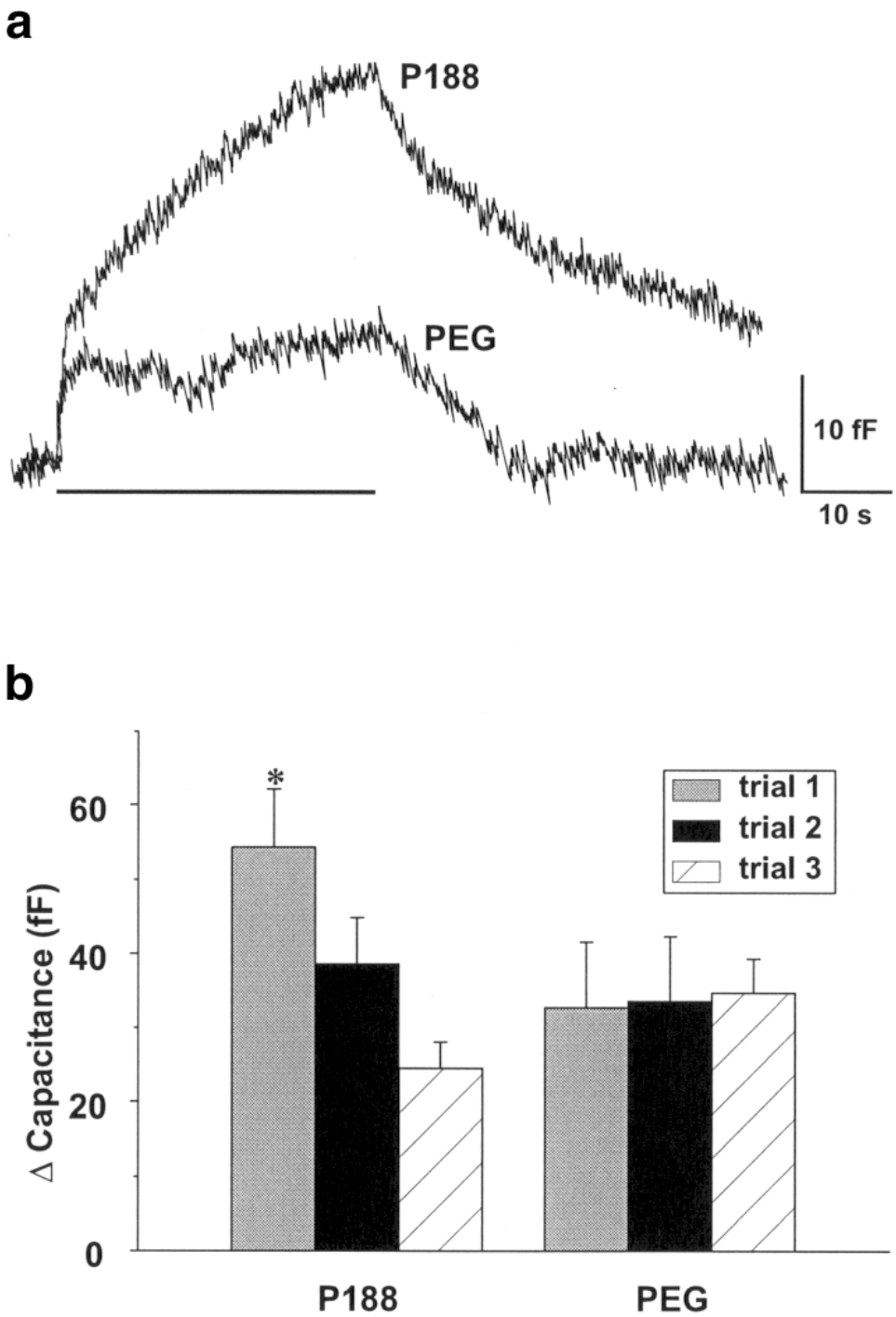

Figure 4. Increases in whole-cell capacitance by P188 and PEG. (a) Superimposed traces of continuous changes in capacitance over time of bovine adrenal chromaffin cells in response to perfusion (bar) of P188 (100 μM) and PEG (mw 8, 400 100 μM). Baseline capacitance is 5.1 ± 0.28 pF (SE, n=8). Traces have been superimposed so that baseline capacitance values and stimulation onsets overlap. **(b)** Mean changes in capacitance of bovine adrenal chromaffin cells in response to P188 and PEG and plotted as a function of stimulus number. Each bar represents average of 3–5 trials. Error bar is standard error of the mean. All mean capacitance increases following P188 or PEG perfusion are significantly greater ($p<0.05$) than control alone by ANOVA for repeated measures with post hoc comparisons and correction for multiple comparisons. Asterisk shows that P188 perfusion induce significantly greater ($p<0.05$) capacitance increase compared with PEG perfusion by ANOVA. Note that repeated application of P188 induced progressively (and significantly) smaller capacitance increases, but repeated applications of PEG do not.

Fig. 5

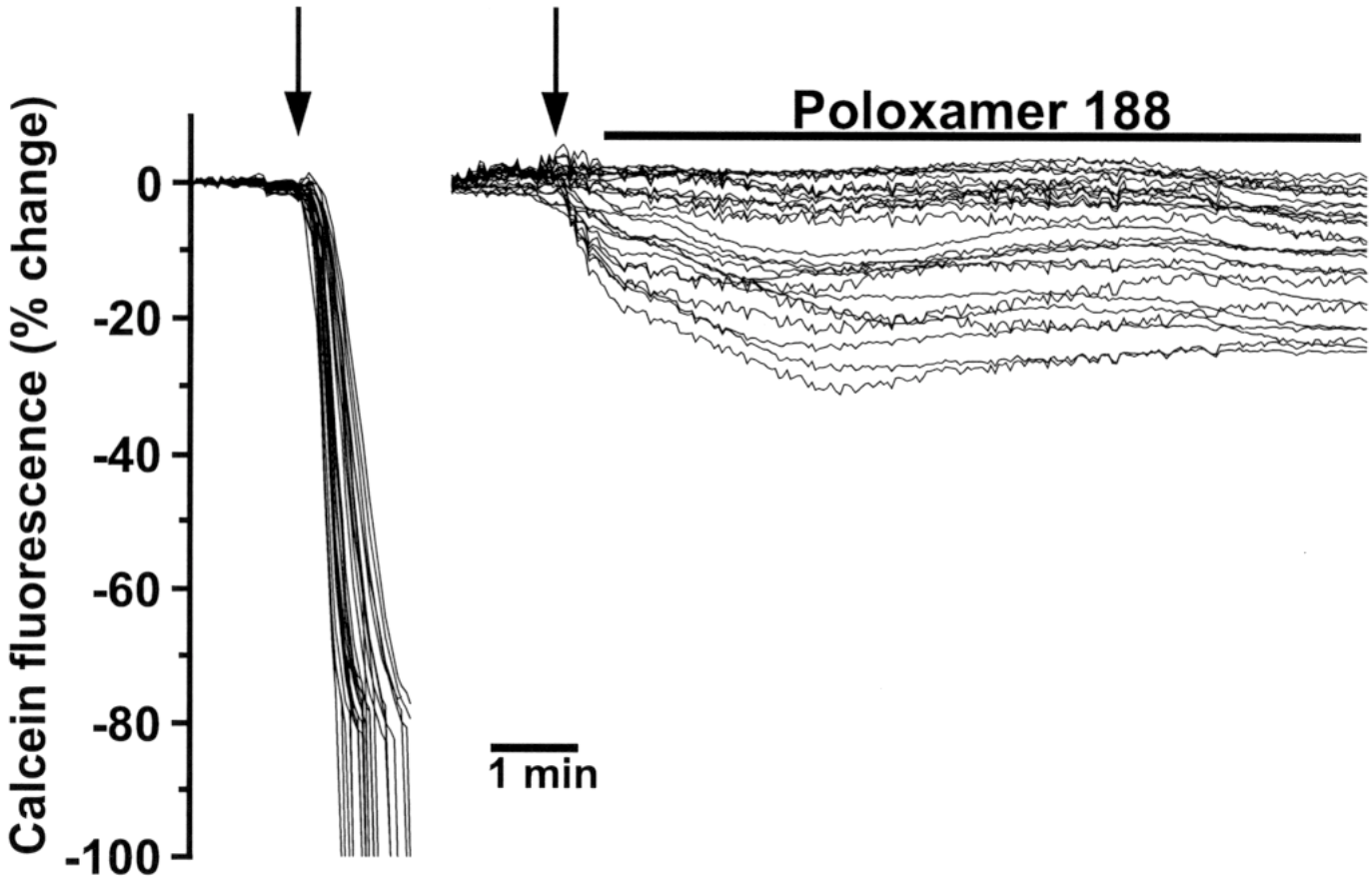

Figure 5. P188 arrests electroporation-induced loss of intracellular contents. Montage of superimposed plots of electroporation-induced changes in intracellular calcein fluorescence of hippocampal neurons in the presence (right panel) and absence (left panel) of P188 (100 μM, bar). Electroporation train (5 Hz, 1 s) delivered at arrows. For each cell, fluorescence change is plotted as a percentage of baseline.

Fig. 6

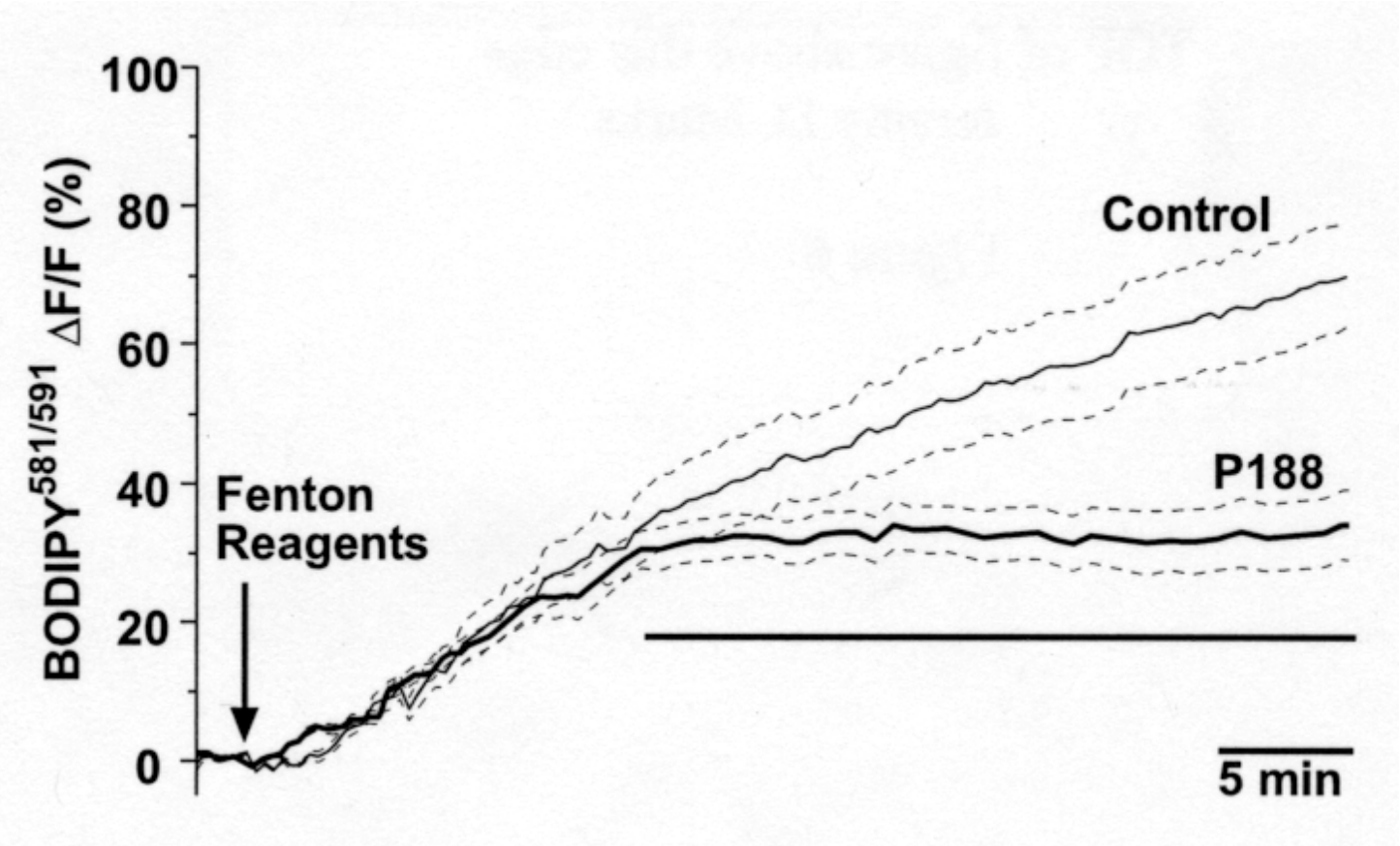

Figure 6. P188 blocks lipid peroxidation induced by Fenton reagents. Superimposed traces of changes in oxidized C11-BODIPY$^{581/591}$ fluorescence (excitation 480 nm, emission 525 nm) induced by perfusion of Fe^{2+} (as ferrous ammonium sulfate, 200 μM) and H_2O_2 (1 mM) in the absence of P188 and following its addition. Fluorescence changes are plotted as percent change from baseline. Solid line represents mean change and dotted lines represent standard errors of the mean, calculated on an image-by-image basis. Control traces shows data from six neurons. P188 trace shows data from nine neurons.

Fig. 7

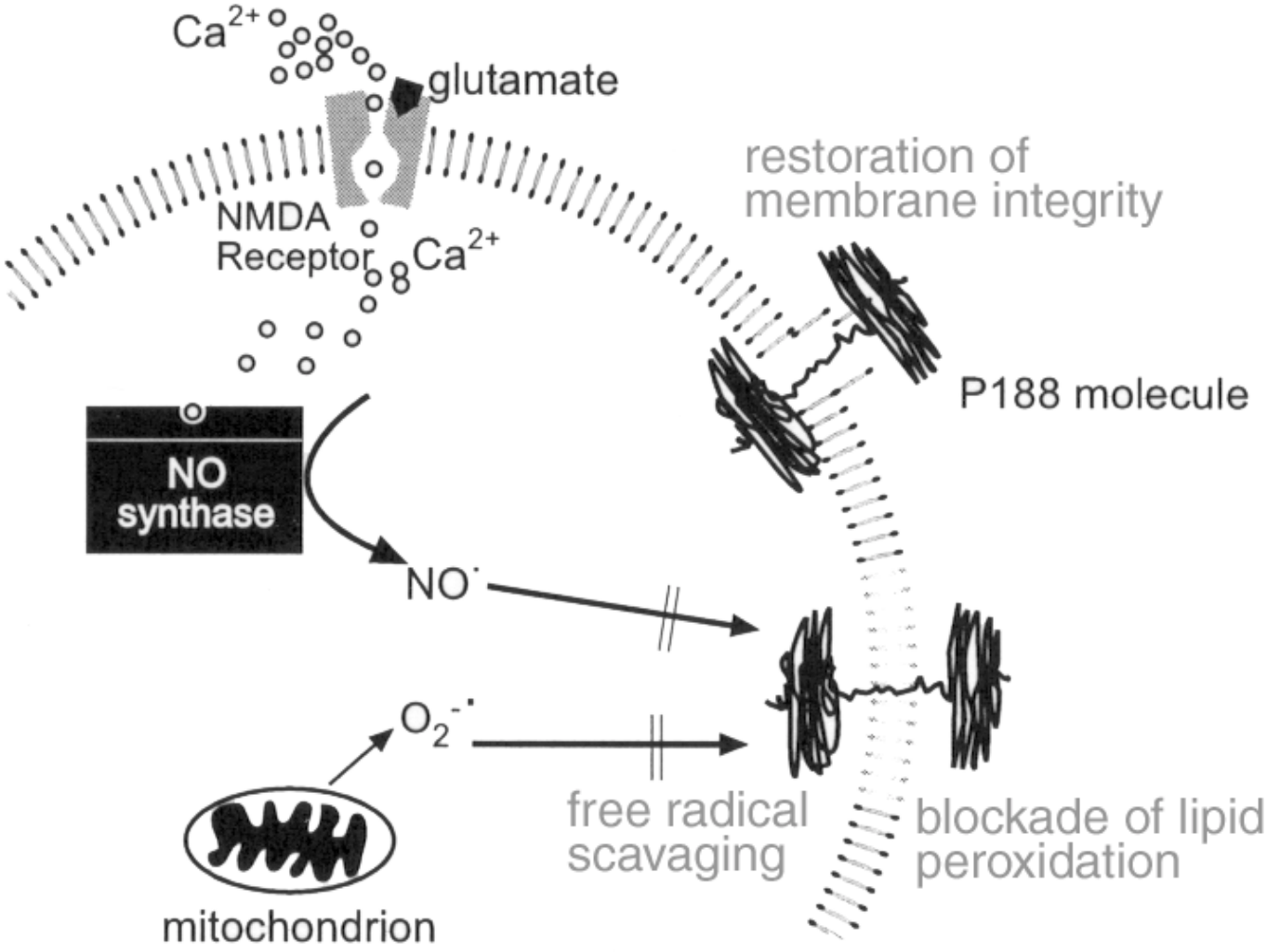

Figure 7. Schematic of membrane-targeted mechanisms that cause NMDA -induced neuronal death and the actions of P188 on the plasma membrane. Two P188 molecules are shown inserted into the membrane during NMDA receptor activation. One molecule is depicted physically sealing a breach of the plasma membrane, as occurs following electroporation. The other molecule is shown scavenging NMDA-induced production of reactive oxygen species an d directly blocking lipid peroxidation.